Research Square

Preprints are preliminary reports that have not undergone peer review.
They should not be considered conclusive, used to inform clinical practice,
or referenced by the media as validated information.

Sensitivity Analysis of the Elastic Parameters of an Industrial Robot with Triaxial Flexibility within its Workspace

Hugo Dantinne

hugo.dantinne@umons.ac.be

University of Mons

Valentin Dambly

IDEKO Research Center

Edouard Riviere-Lorphevre

University of Mons

Bryan Olivier

University of Mons

Research Article

Keywords: Sensitivity Analysis, Parameter Identifiability, Robotics, Multibody Modelling

Posted Date: May 19th, 2026

DOI: https://doi.org/10.21203/rs.3.rs-9680279/v1

License: This work is licensed under a Creative Commons Attribution 4.0 International License.
Read Full License

Additional Declarations: No competing interests reported.

The 8th International Conference on Multibody System Dynamics
June 16-19, 2026, Seville, Spain

Sensitivity Analysis of the Elastic Parameters of an Industrial Robot with Triaxial Flexibility within its Workspace

Hugo Dantinne[*], **Valentin Dambly**[#,+], **Edouard Riviere-Lorphevre**[#], **Bryan Olivier**[*]

[*] Department of Theoretical Mechanics, Dynamics and Vibrations
University of Mons
20 Place du Parc, 7000, Mons
hugo.dantinne@umons.ac.be
bryan.olivier@umons.ac.be

[#] Department of Machine Design and Production Engineering
University of Mons
20 Place du Parc, 7000, Mons
valentin.dambly@umons.ac.be
edouard.rivierelorphevre@umons.ac.be

[+] IDEKO
Research Center
Arriaga Industrialdea 2,
E-20870 ELGOIBAR (Gipuzkoa)
vdambly@ideko.es

ABSTRACT

Industrial robots used for machining operations exhibit lower stiffness than conventional machining machines, making accurate identification of their elastic parameters essential for predictive modeling and compensation. Virtual Joint Modeling (VJM) with triaxial flexibility offers high-fidelity compliance representation, but introduces up to 44 stiffness and damping parameters whose influence on the system response remains largely unknown. This paper presents a sensitivity analysis of these elastic parameters for a flexible 6 degrees of freedom industrial robot incorporating joint flexibility, link compliance, ground flexibility, and a dynamic vibration absorber, conducted across 351 configurations spanning position and tool orientation within the operational workspace. Both local (One-At-a-Time) and global (Improved Morris and Sobol) sensitivity methods are applied, using a cost function based on Frequency Response Functions (FRFs) as performance indicator. A Kriging metamodel is developed and validated to enable variance-based analysis at tractable computational cost. Three key findings emerge from this study. First, stiffness parameters dominate the system response while damping and DVA parameters have negligible influence and may be assigned fixed values during identification. Second, a parameter identified as influential remains influential across the configurations studied, a result with direct practical implications for pose-independent identification strategies. Third, variance decomposition reveals predominantly additive behavior with weak pairwise interactions, with the exception of geometrically coupled joint pairs, whose interaction effects reach up to 28%. Together, these findings support a multipass parameter identification strategy with dimensionality reduction, improved robustness of FRF-based model updating, and physically grounded justification for the use of triaxial over simpler VJM formulations.

Keywords : Sensitivity Analysis, Parameter Identifiability, Robotics, Multibody Modelling

Acknowledgements

The authors would like to acknowledge the Belgian National Fund for Scientific Research (FNRS-FRS) and the UMONS Risk Institute for the grant allocated to H. Dantinne.

1 Introduction

In recent decades, Industrial Robots (IRs) have increasingly been employed across a variety of tasks, including painting, material handling, and machining. Their application in machining is particularly attractive to industry due to several advantages: lower cost compared to dedicated machining equipment, generally larger workspaces, and greater adaptability within production lines [1, 2]. These characteristics are especially valuable in a rapidly evolving market where customization and flexibility are becoming increasingly

important. However, these advantages come at a cost. Overall, IRs are less rigid than that of the conventional CNC machine tools, it has been determined that the general stiffness of the robots is 50 times lower. This causes deflection of the whole robot, and consequently the tool tip during machining operations, as well as more vibrations. Consequently, the lack of rigidity due to the open loop structure leads to instabilities, called chatter. These instabilities lead to excessive wear of the tool and degraded surface finish of the workpiece. The second main consequence of this flexibility is the deflection induced in the robot due to the cutting forces, preventing the achievement of the planned tolerances [1].

To mitigate these limitations, various methodologies have been developed and are generally categorized into two primary classifications: online [3] and offline [4] strategies. Online methods utilize real-time monitoring and control during operation, leveraging external sensors to dynamically correct path deviations and suppress robotic vibrations. Conversely, offline methods employ high-fidelity digital twins of the robotic system and process parameters to predict instabilities and pre-emptively compensate for mechanical deflections. This approach necessitates the development of numerical models that accurately reflect the physical robot's behaviour, requiring a strategic balance between model complexity and computational efficiency.

In modeling robotic compliance, two primary factors are typically considered: joint flexibility and link flexibility, with the former generally exerting a more significant influence on the general behaviour of the system [5]. Various approaches have been proposed to characterize joint flexibility; however, Virtual Joint Modeling (VJM) remains the most prevalent framework. The fundamental principle of VJM involves augmenting the kinematic chain with localized spring-damper pairs at the joints, where each pair represents a specific degree of freedom. Depending on the required fidelity, VJM is typically implemented through three primary methodologies: Single VJM [6], Complete VJM [7], and Triaxial Flexibility models [5], which account for non-diagonal elements in the joint compliance matrix, offering higher fidelity at the cost of increased parametric dimensionality, with a limited increase of parameters relative to a Complete VJM model. This higher fidelity comes from the fact that robots are not infinitely stiff around the axis perpendicular of the axis of rotation of the motors, due to deformations in the transmission for instance. These variants offer a tiered approach to modeling, presenting a direct correlation between structural complexity and the accuracy of the resulting compliance matrix.

To identify the parameters of equivalent springs, researchers typically employ laser tracking systems to measure static deflections at the end-effector or individual joints under known mass loads [8, 9]. While laser trackers provide high precision, their prohibitive cost has motivated the development of alternative metrology frameworks. These include the use of digital micrometers [10], 3D measuring systems [11], and vision-based systems utilizing AruCo markers [12, 13]. Beyond static analysis, the literature also describes dynamic identification via the alignment of experimental Frequency Response Functions (FRFs) with analytical models [14].

Because these measurement techniques do not yield stiffness and damping coefficients directly, the identification process is formulated as an optimization problem. Various computational strategies have been implemented to resolve these parameters, ranging from metaheuristic approaches like genetic algorithms [14] to machine learning architectures such as Convolutional Neural Networks (CNNs) [15], Random Forests [16], and Gaussian Process Regression [17].

The computational burden of these identification methods scales significantly with the degrees of freedom (DOF) and the complexity of the stiffness model. For instance, a 6-DOF industrial robot utilizing tri-axial flexibility modeling requires the identification of at least 36 parameters. Furthermore, since robot compliance is inherently pose-dependent (often fluctuating across the workspace due to model simplifications and geometric non-linearities) recurrent execution of these expensive optimization routines becomes necessary.

To mitigate this computational overhead, dimensionality reduction is essential. Sensitivity analysis provides a robust framework for identifying parameters with negligible influence on the end-effector displacement, allowing them to be fixed during optimization without compromising accuracy. This facilitates the implementation of multi-pass optimization algorithms, where a subset of high-impact parameters is identified in the primary stage, followed by the refinement of secondary parameters. Despite the potential for efficiency gains, the literature currently lacks a comprehensive sensitivity analysis of pose-dependent stiffness and damping parameters in industrial robots within VJM-based identification frameworks.

The specific contributions of this work are :

- A comprehensive sensitivity analysis of a triaxial VJM model with 44 parameters
- A systematic workspace-wide evaluation across 351 configurations covering both position and tool orientation effects
- Evidence that parameter interactions are predominantly weak and additive for this cost function except for geometrically coupled joint pairs
- A validated Kriging metamodel strategy enabling variance-based analysis at tractable computational cost

The preceding discussion underscores the necessity of a comprehensive sensitivity analysis regarding the robotic stiffness and damping parameters across the entire operational workspace. The remainder of this article is structured as follows: Section 2 outlines the robotic model, encompassing the fundamental kinematics and dynamics, followed by a derivation of the flexibility modeling and the generation of Frequency Response Functions (FRFs). Section 3 initiates the sensitivity study using a local approach, specifically the One-at-a-Time (OAT) method. Finally, Section 4 explores advanced global sensitivity analysis techniques, employing the Morris Method to identify influential parameters. This section further details the development of a Kriging metamodel used to compute first-order, second-order, and total-effect Sobol indices indices to quantify more complex parameter interactions.

2 Model of the Robot

This section presents the robot model used for the sensitivity analysis. In the context of elastic parameter identification, the model takes the stiffness and damping coefficients, as well as the joint angular values, as input parameters, while the outputs are the corresponding Frequency Response Functions (FRFs). The kinematic robot model described herein is the model previously developed by Huynh et al. [5] enhanced with link flexibility. The model employed in the actual work is constructed using data provided by the robot manufacturer under a non-disclosure agreement (NDA). Consequently, the nominal values of inertial properties, masses, and geometric dimensions are not disclosed. Nevertheless, representative and physically meaningful values can be found in the work of Huynh et al. [18], which provides sufficient reference for understanding the modeling approach adopted in this study.

The kinematics of the robot, from the base O_{Base} to the end effector (EE) O_{EE} (Figure 1) can be constructed using the Denavit-Hartenberg convention [19] given in Table 1, using homogeneous transformation matrices. The robot is built through the use of minimal coordinates, and the 6 DOF are given in Figure 1 by the notation q_i.

Frame O_0 is translated by a distance l_{Base} along the Z-axis of frame O_{Base}. The end-effector frame O_{EE} is translated from frame O_6 by a distance l_{EE} along its local Z-axis. Finally, the tool-holder frame O_{Tool} is positioned with respect to frame O_{EE} by offsets $l_{\text{Tool},x}$ along the X-axis and $l_{\text{Tool},z}$ along the Z-axis, followed by a rotation of θ_{Tool} about the transported Y-axis.

Table 1: Stäubli TX200 DH parameters values

DOF_i	a_i [m]	α_i [rad]	d_i [m]	θ_i [rad]
1	0.25	-$\pi/2$	0	θ_1
2	0.95	0	0	θ_2
3	0	$\pi/2$	0	θ_3
4	0	-$\pi/2$	0.8	θ_4
5	0	$\pi/2$	0	θ_5
6	0	0	0	θ_6

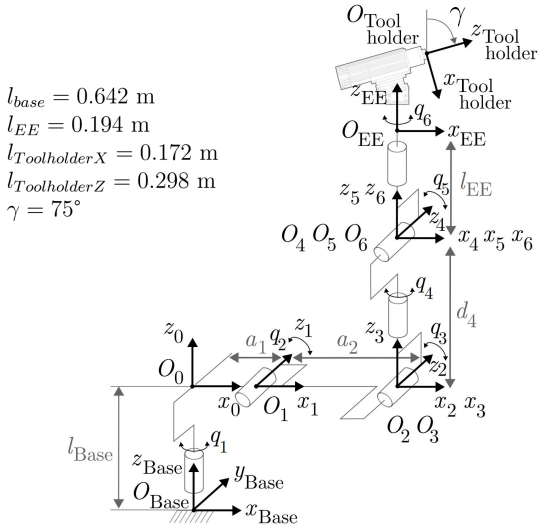


Fig. 1: Illustration of the kinematics of the Stäubli TX200

When the kinematics of the robot are defined and the inertial properties of the robot are set, the transational and rotational velocities can be calculated for each body with time derivation of the homogeneous transformation matrices. Transational and rotational accelerations are given by the time derivatives of the velocities. The method for the calculation of the dynamics and motion of the system is given in [20].

2.1 Robot Flexibility

The robot flexibility is composed of link flexibilities and joint flexibilities, the latter being the most impactful. In the model used here, the link flexibility is modelled with the co-rotational approach [21] as explained in Huynh's Ph.D. thesis [5] for the arm and forearm of the robot. The other bodies being non-elongated, their flexibility was considered negligible.

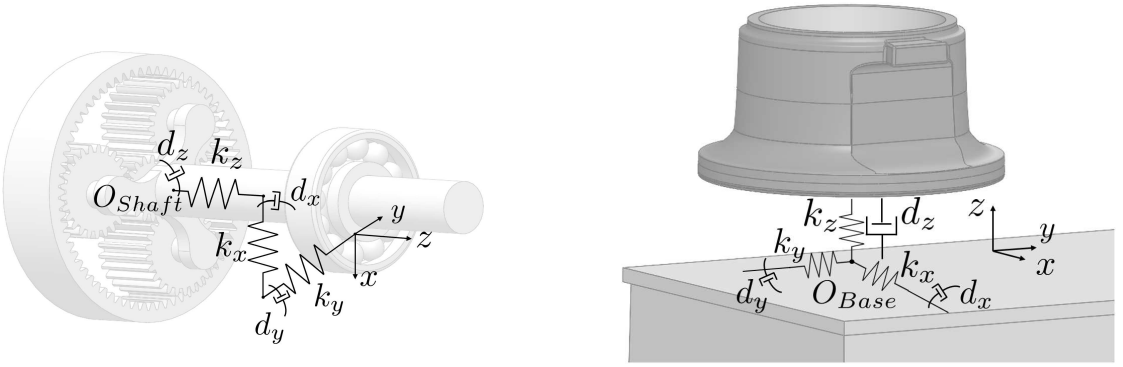
Joint flexibility was modelled through Virtual Joint Modelling (VJM) [7]. VJM is a way of modelling robot stiffness and compliance by representing joints as damper-spring pairs with equivalent elastic properties. Different levels of VJM exist. First, a single pair of spring-damper around the rotation axis of the joint, making what is called the transmission flexibility exists [6]. Another type of joint modelling is the full one [7], having 6 pairs of spring-dampers, for the 3 rotational and 3 translational flexibilities. As its name states, it is the most complete model, however, it is more computationally costly. Thus, an *in between* model, called tri-axial flexibility has been developed and is used in the model of the robot [5]. This model uses, for each of the 6 joints of the robot, 3 pairs of torsional spring-dampers, one for each rotation in space. Figure 2a illustrates the triaxial flexibility for a joint of the robot.

In the robot's modelling, their impact is an elastic force for each element. This elastic force makes an action and a reaction between the shaft of the motor and following body. The action (torque $\mathcal{M}$) applied at the centre of gravity G of a body *j* is given by Equation 1 and its reaction is applied on the other body.

$$\mathcal{M}_{\mathbf{G,j}} = (\mathbf{K_i}.(\mathbf{q_{ref,i}} - \mathbf{q_i}) + (\mathbf{D_i}.(\dot{\mathbf{q}}_{\mathbf{ref,i}} - \dot{\mathbf{q}}_{\mathbf{i}})) \tag{1}$$

With :

- $\mathbf{K_i}$: The vector containing stiffness values of parameter *i* in the 3 directions of space
- $\mathbf{D_i}$: The vector containing damping values of parameter *i* in the 3 directions of space



(a) Triaxial flexibility modelling for a joint

(b) Triaxial flexibility modelling for the ground

Fig. 2: Illustration of the triaxial flexibility modelling for a joint and the ground

- $\mathbf{q_{ref,i}}$: Reference value of the position of the degree of freedom linked to that flexibility (if the robot was rigid)
- $\mathbf{\dot{q}_{ref,i}}$: Reference value of the velocity of the degree of freedom linked to that flexibility (if the robot was rigid)
- $\mathbf{q_i}$: Value of the position of the degree of freedom linked to that flexibility
- $\mathbf{\dot{q}_i}$: Value of the velocity of the degree of freedom linked to that flexibility

Those $\mathbf{k_i}$ and $\mathbf{d_i}$ are the parameters on which the sensitivity analysis is performed, this means 6 (n_{joints}) times 6 (parameters per joint) = 36 parameters. However, 8 other parameters are added to the study. Six are the ground flexibility, shown on Figure 2b, modelled like the joint flexibility, with the difference of the flexibility around the Z axis (direction of gravity) is a translation, and the two remaining are k_{DVA} and d_{DVA}, the stiffness and damping linked to the Damper Vibration Absorber (DVA) situated in the robot [5].

2.2 Generation of Frequency Response Functions

The system output considered for the sensitivity analysis is defined through a cost function that quantifies the effect of perturbations compared to the nominal set of elastic parameters on the system's Frequency Response Functions (FRFs). Consequently, an accurate and efficient method for generating these FRFs is required. The approach adopted in this work is based on the method proposed by Huynh et al. [22]. Briefly, the mass **M**, damping **C**, and stiffness **K** matrices are first computed by linearizing the robot model around the configuration under study, using the specified elastic and inertial parameters. Simultaneously, an external force applied at the robot tool tip is mapped into equivalent joint-space torques. Under these conditions, the resulting joint-space oscillations $\mathbf{\Delta q}$, where q denotes the system degrees of freedom, are obtained using Equation 2 for each excitation pulsation ω_k of interest. Finally, the 10 displacements at the FRF measurement points, illustrated in Figure 3, are computed via forward kinematics from the joint-space oscillations. These displacements are transformed into accelerations in the frequency domain. The measurements are done at each measurement point in the 3 dimensions of space for three different excitations at the Tool Tip, one for each direction of space. One of the generated FRFs of the robot is given for illustration to the reader at figure 4.

$$\mathbf{\Delta q}(\omega_k) = (-\mathbf{M}_0.\omega_k^2 + j\omega_k\mathbf{C}_0 + \mathbf{K}_0)^{-1}\{\tau\}_{Base} \tag{2}$$

As the goal of this paper is to perform the sensitivity analysis in the workspace of the robot, 27 points were chosen in a rectangular parallelepiped with a square base of 800 mm by side and a height of 400 mm and the centre in [0.0, -1671.5, 0.642] mm. This measurement space is divided in three planes, with 9 measurement points in each one of them, as found in the literature [23], this is shown in Figure 5. The first idea was to

perform it in a cube of 800 mm by side, however, most of the orientations wanted in the top plane cannot be attained within the dexterous workspace of the robot. Speaking of orientations, the goal was also to assess if the relative importance of the parameters is changed with the orientation of the tool. For this, 13 different orientations of the spindle have been chosen, as shown in Figure 6. For rotations around the X and Y axis, the red lines represent how the spindle is directed, and the angular values of the spindle are, in degrees [-60, -30, 0, 30, 60] and [-90, -45, 0, 45, 90]. For the rotation around the Z axis, the green line represents the orientation of the wrist of the robot, the spindle being directed downwards, the angular domain is [-70, -35, 0, 35, 70], in degrees. At first, a [-90, 90] domain was chosen for each of the orientation directions of the tool, however, for X and Z rotations, numerous limitations came from the physical joint limits of the robot. Combining the 27 points and the 13 orientations for each other, there is a total of 351 positions in which the robot is analysed.

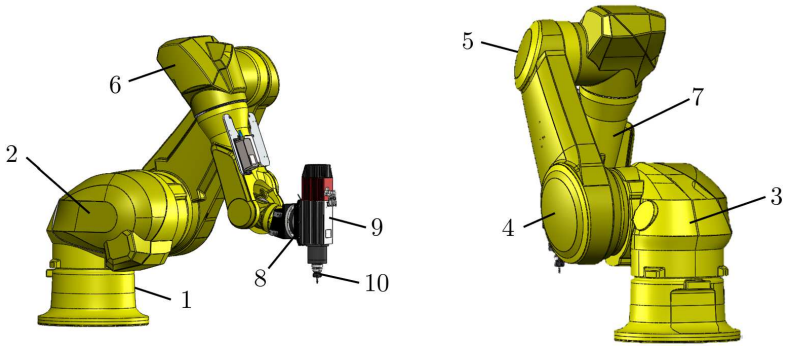


Fig. 3: Distribution of the measurement points for accelerometers on the robot

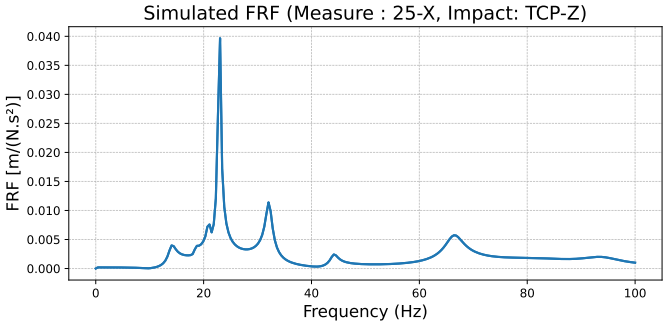


Fig. 4: Generated FRF for measurement at point 25 in the X direction for an impact in the Z direction at the TCP

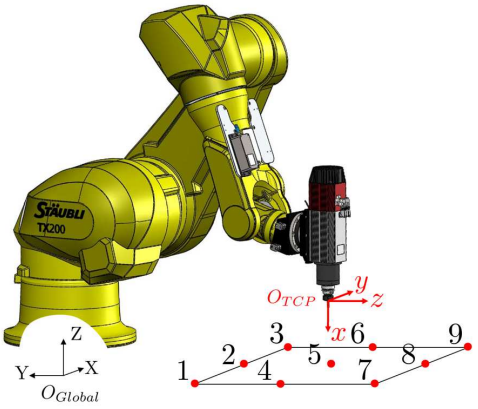


Fig. 5: Points of the robot in the inferior plan analysed

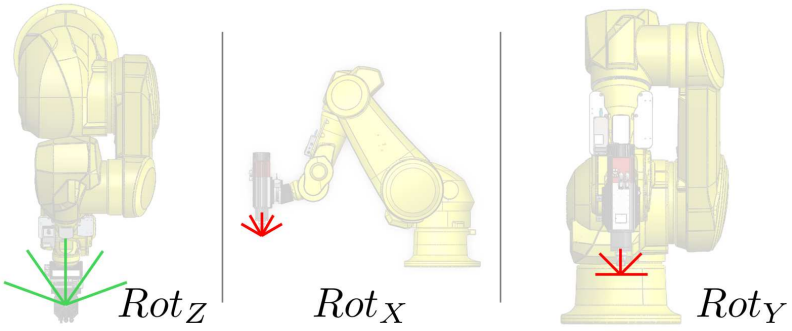


Fig. 6: Orientations for a point of the robot

3 Local Methods

Local sensitivity analysis methods aim to evaluate the effect of perturbations in input variables on the output of a system around a nominal or reference point in the parameter space. One of the most widely used local sensitivity methods in engineering is the One-At-a-Time (OAT) approach [24], in which each input parameter is varied individually while the others are held constant. This method is described in greater detail in the following subsection. Local methods are deterministic and typically rely on partial derivatives or finite perturbations to quantify the influence of individual parameters on the system response. Due to their low computational cost, they are particularly well suited for models with a large number of input parameters [25]. However, they are limiting as they do not show the dependencies between variables. Other local methods, such as *Cobweb visualisation* and *pairwise visualisation*, are not considered in this work due to the large number of parameters involved, which would make their interpretation difficult.

3.1 One-at-a-time

The first thing to do is to define how the influence of a change in the input parameters will affect the output value of the model, and how the output value (a cost function) will be calculated. This cost function will remain the same for the following analysis, the Morris Analysis.

As the goal is to assess the sensitivity of the model, a first set of nominal parameters had to be chosen. The set of parameters chosen was the one determined by Huynh [5] and is the one used in his model, given in Table 2. It should be noted that for these values, the axis given are local axis.

Table 2: Stäubli TX200 K and D parameters values [5]

	Joint Stiffness	Unit		Joint Damping	Unit
K_1 (x-y-z)	$13.05e^6$ - $16.99e^6$ - $2.29e^6$	[Nm/rad]	D_1 (x-y-z)	$0.12e^3$ - $0.2e^3$ - $4.56e^3$	[Nm.s/rad]
K_2 (x-y-z)	$4.08e^6$ - $19.94e^6$ - $8.60e^6$	[Nm/rad]	D_2 (x-y-z)	$0.98e^3$ - $2.16e^3$ - $5.01e^3$	[Nm.s/rad]
K_3 (x-y-z)	$18.84e^6$ - $2.95e^6$ - $2.76e^6$	[Nm/rad]	D_3 (x-y-z)	$2.63e^3$ - $0.10e^3$ - $2.51e^3$	[Nm.s/rad]
K_4 (x-y-z)	2.96 e^6 - 2.26 e^6 - 3.14 e^6	[Nm/rad]	D_4 (x-y-z)	$0.30e^3$ - $1.03e^3$ - $0.01e^3$	[Nm.s/rad]
K_5 (x-y-z)	$2.13e^6$ - $0.94e^6$ - $0.19e^6$	[Nm/rad]	D_5 (x-y-z)	$0.03e^3$ - $0.03e^3$ - $0.01e^3$	[Nm.s/rad]
K_6 (x-y-z)	$14.84e^6$ - $8.28e^6$ - $0.91e^6$	[Nm/rad]	D_6 (x-y-z)	$0.01e^3$ - $0.01e^3$ - $0.01e^3$	[Nm.s/rad]
K_{ground} (x-y)	$20.27e^6$ - $48.10e^6$	[Nm/rad]	D_{ground} (x-y)	$50.52e^3$ - $54.39e^3$	[Nm.s/rad]
K_{ground} (z)	32.12 e^6	[N/m]	D_{ground} (z)	5.00 e^3	[N.s/m]
K_{DVA}	67.00 e^3	[Nm/rad]	D_{DVA}	$0.01e^3$	[Nm.s/rad]

To assess the impact of a modifications in the set of parameters, the following cost function J (Equation 3) was used. This cost function sums the difference over all the FRFs generated and the frequency domain studied of the squared difference between the nominal and modified FRFs. This type of cost function is typically used in the literature, for example, see [26].

$$J = \sum_{i=0}^{n_{FRF}} \sum_{\omega_k=0}^{\omega_{max}} (20.log(H_{i,j,nom}) - 20.log(H_{i,j,mod}))^2 . \frac{1}{10^5} \tag{3}$$

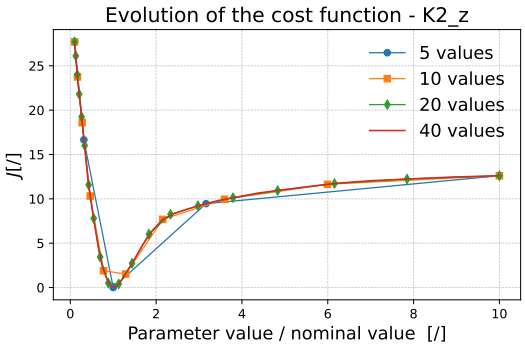
With :

- n_{FRF} : The total number of FRFs generated (10 measurement points in the 3 directions of space, each for an impact at the TCP in the 3 directions of space - 90 in total)
- $\omega_{max} = 2.\pi.f_{max}$: The maximum value of the pulsation of the domain studied (0-100 Hz)
- H_{nom} : FRF generated with the nominal set of parameters
- H_{mod} : FRF generated with the modified set of parameters
- $\frac{1}{10^5}$: Scaling factor to avoid huge values of the cost function, making it easier to read

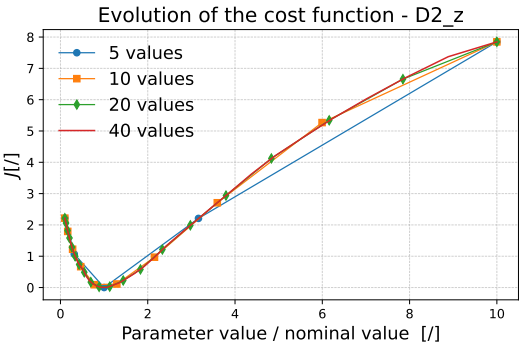
Now, an important aspect is the domain of the variations of the parameters and the distribution used. As the nominal parameters are set in typical values, it has been chosen to study their sensitivity on 2 orders of magnitude, which means that the domain of a parameter is given by $[0.1, 10]$ times the value of the parameter. As it is as important to study what happens under the nominal value than that of what happens over, the distribution of the values follows a logarithmic distribution.

In order to determine the optimal number of points to evaluate for each parameter, a first run of the OAT on a position of the robot was conducted for 5, 10, 20 and 40 points of the domain. The results can be observed in Figure 7, for a stiffness and a damping parameters.

Based on the analysis of this graph, a discretization of 10 evaluation points represents an appropriate compromise between computational cost and accuracy. Using only 5 evaluation points over the entire parameter domain is overly coarse and fails to capture the parameter evolution with sufficient fidelity. In contrast, 10 evaluation points yield results that are in close agreement with those obtained using 40 points, except in the vicinity of the nominal values of the stiffness parameters. Nevertheless, the sensitivity in this region remains small compared to the variations observed for larger deviations from the nominal values, and therefore does not significantly affect the identification of the most influential system parameters. Increasing the number of evaluation points to 20 would slightly improve accuracy but would also double the computational time. This increase becomes prohibitive when analyzing a large number of poses as the total computational time would go from 10 to 20 days. Consequently, OAT analysis for all poses of the robot are conducted using



(a) Different discretization - $K1_z$



(b) Different discretization - $D1_z$

Fig. 7: Evolution of cost function with different numbers of evaluations of the cost function J

10 evaluation points per parameter. Given that 44 parameters are investigated, it is not feasible to show the results for each parameter and each pose within this article.

However, the following pictures (8, 9, 10) show the results for position 170 (Values at the joints in degrees : -90.01, 22.80, 106.11, 0.00, -23.89, 0.00), being the position where the TCP is in the middle of the analysed volume with the tool in the vertical direction. Those results show that, for the stiffnesses of the model, they follow the same trend, when the value is decreased, the system becomes more and more flexible, and when the system becomes stiffer, this has an influence on the FRFs, until a certain point where the stiffness is so high that being more stiff does not change anything anymore in the studied domain. This is true with the exception of the $K5_z$, as it goes through a maximum before stabilization. This might be due to its lower value compared to the other stiffnesses. The explanation can be explained visually, when increasing the value of this stiffness parameter, one of the peaks of the FRFs grows in amplitude and then goes out of the studied domain (which explains the maximum reached on the graph). Overall, stiffnesses around the x axis have the least impact (with the exception of the ground). Stiffnesses around the y axis are more sensitive for lower values of the parameters, but at higher values, they tend to stabilize at a lower cost function that the stiffnesses around z. As expected, the evolution of the damping values follows an overall trend approximating a flattened V-shape. Their impact is more important around the z axis.

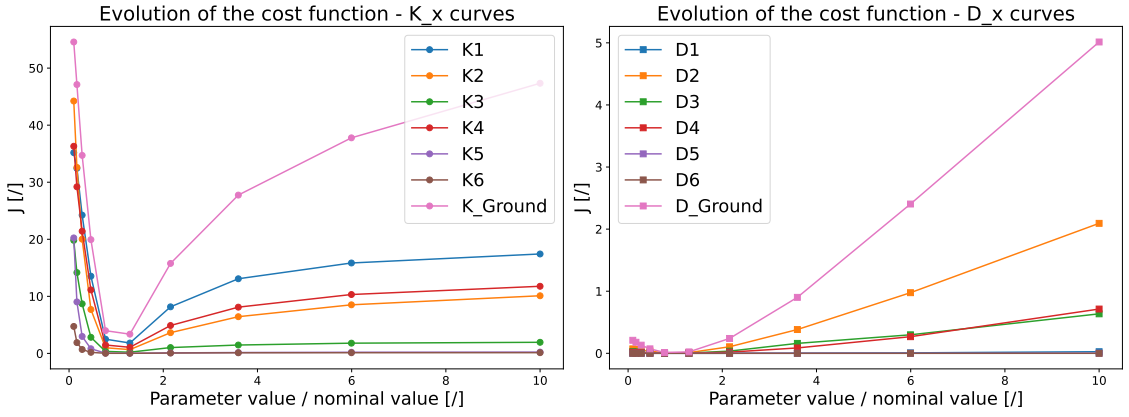


Fig. 8: Evolution of the cost function J with the values of parameters around X - pose 170

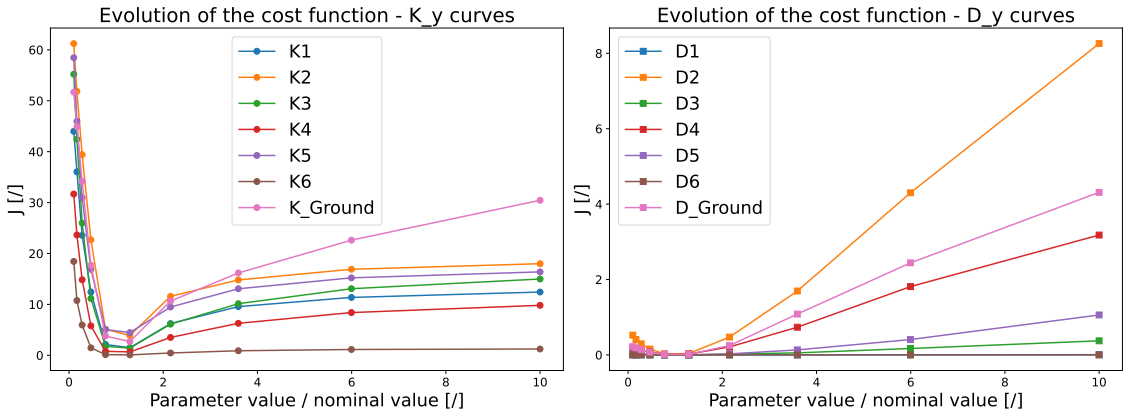


Fig. 9: Evolution of the cost function J with the values of parameters around X - pose 170

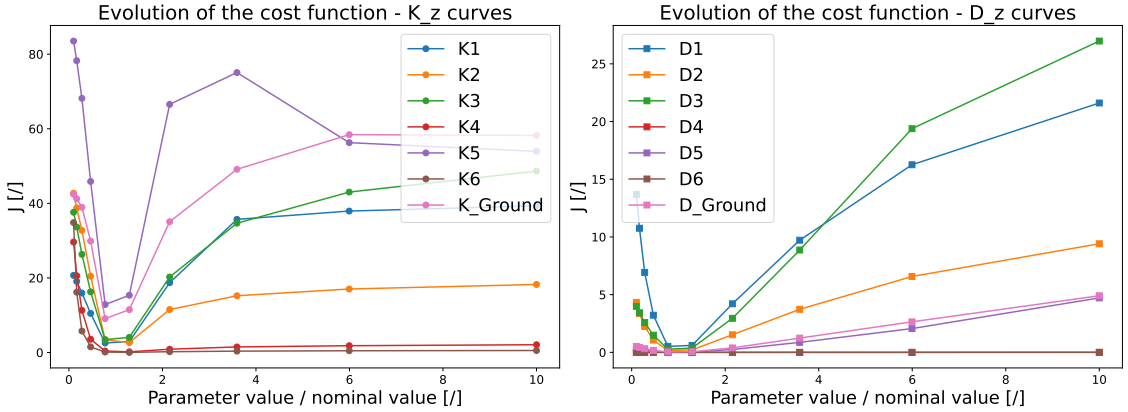


Fig. 10: Evolution of the cost function J with the values of parameters around Z - pose 170

For the parameters of the DVA (Figure 11), the evolution of the damping is similar to the one of the joints, however, the stiffness follows a different trend than that of the joints. For this reason, an analysis in more details had to be made (with 40 evaluations). This trend is quite erratic and shows that, adding no DVA, or with a very small stiffness modifies the FRFs in a constant way, if the parameter is increased, the overall trend is for the FRFs to change more and more after passing by with a local maximum and a local minimum. However, the DVA had been added after observations on experimental FRFs [5]. Consequently, a more detailed investigation of this parameter, as well as its associated damping, is not deemed necessary. Moreover, the cost associated with a change of the value of a parameter is negligible to the ones of the joints and ground.

In order to show the results of pose 170 in a more simple way, the values of the cost function over the studied domain was summed for each parameter and shown on Figure 12. This figure shows that, as seen previously, the most influential parameters are the stiffnesses compared to damping, with the ground and 4th motors (2nd of the wrist) being prominent and that the DVA is not of importance. Figure 13 shows the 20 most influential parameters over the whole workspace (limited to 20 for readability issues, but the trend can be extrapolated). The sum of the cost functions for each parameter was done, and averaged across each plane (see subsection 2.2). The results show that a parameter important in a plane will stay important in another plane, with small variations on the cost function.

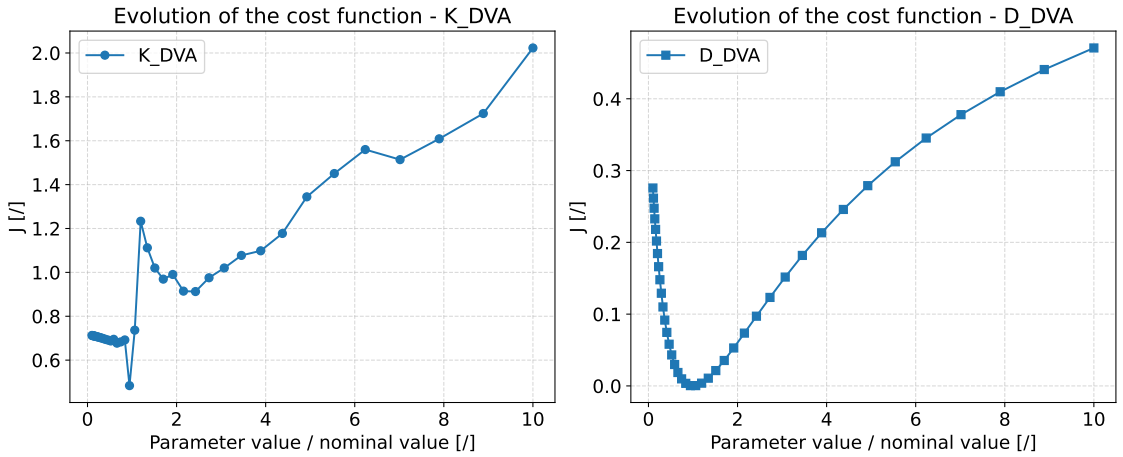


Fig. 11: Evolution of the cost function J with the values of the DVA - pose 170

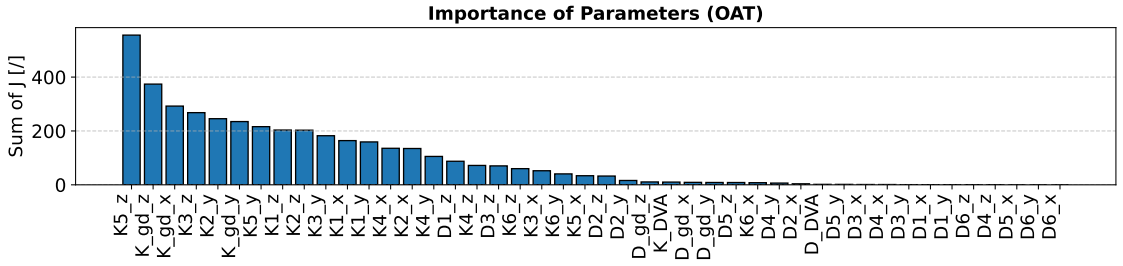


Fig. 12: Sum of the values of cost function J for the parameters - pose 170

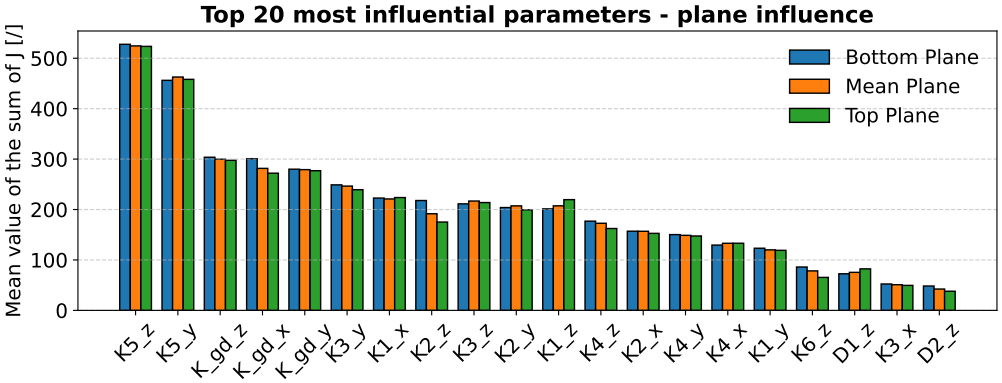


Fig. 13: Most influential parameters over the 3 planes studied

To perform a comprehensive analysis of the space, a comparison was conducted among the nine points in the mean plane with the tool oriented downwards. However, the low number of points across the directions X and Y did not allow to observe tendencies. For this reason, more points were added to the study. Staying in the mean plane, 9 points were used in each direction between 2 extremes. For illustration, on Figure 5, it would mean that for X, 9 equidistant points are created between points 4 and 6 (5 being the mean point of the 9). The same can be applied for the Y direction. The results from these studies are given in Figures

14 and 15. Those results show some specific tendencies. The most influential parameters identified at the central pose remain consistently influential across all nine positions, with limited variation in their relative ranking

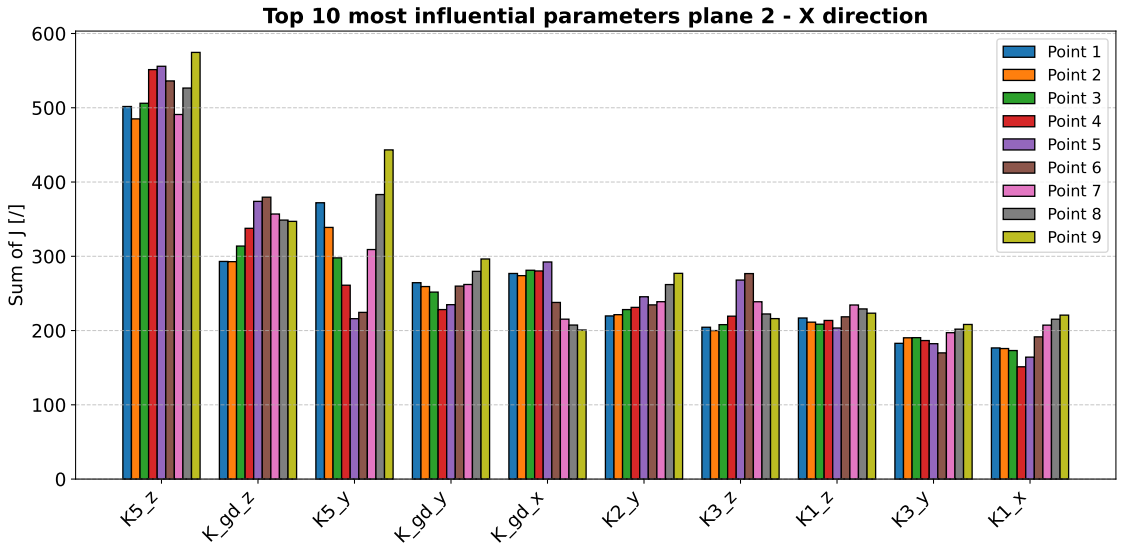


Fig. 14: Most influential parameters - Mean plane - X evolution - OAT

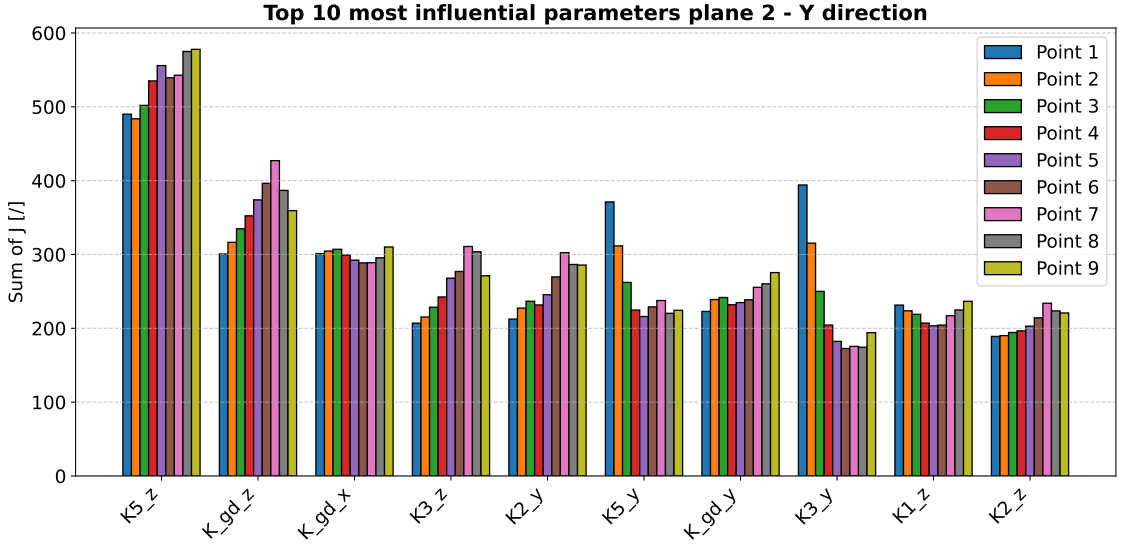


Fig. 15: Most influential parameters - Mean plane - Y evolution - OAT

The study was also conducted for the orientations around the central TCP position (pose 170). When looking at the evolution in around the 3 axes of space (see the values given in the generation of FRFs section). For example, for the axis Y (Figure 5), no real tendency was found, except for $K5_y$, which is less sensitive when getting closer to a 0° orientation (Figure 16). The values for the orientations are reminded here [-90, -45, 0, 45, 90] in degrees. However, by looking for different points, it seems that the central orientation point (tool downwards) is the least sensitive to changes. This observation is marginal and negligible so will have no visible effect on the identification of the parameters. For the example given in this paragraph, the value of the sum of the cost functions for all parameters in the different orientations is respectively [2890, 2808, 2736, 3165, 2901]. The middle value being the 0° orientation.

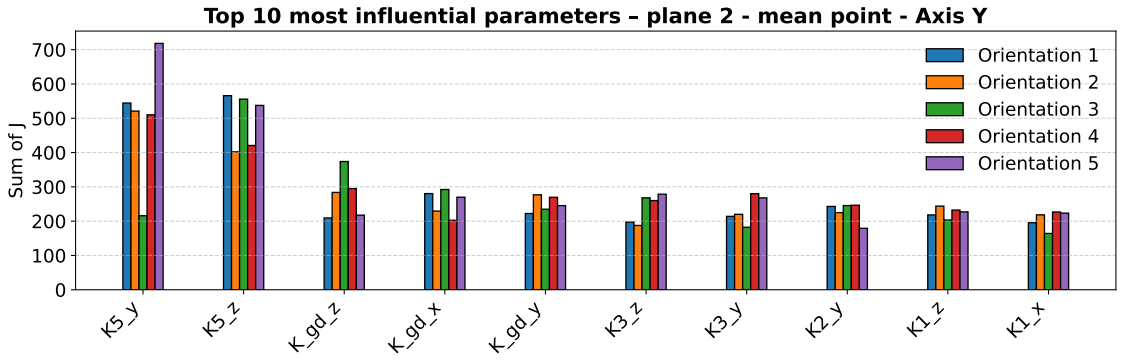


Fig. 16: Most influential parameters - comparison for the orientations around Y for center point of the mean plane

The objective of this section is primarily to provide a qualitative interpretation of the sensitivity trends observed across the parameter space. The results indicate that stiffness parameters exert a significantly greater influence on the system response than damping parameters. In particular, the stiffness associated with the ground also appears to play a non-negligible role. Furthermore, the analysis suggests that flexibilities in directions perpendicular to the motor axis contribute meaningfully to the overall behavior of the system. At the same time, no clear global trend could be identified regarding the influence of individual parameters across all spatial positions and tool orientations, highlighting the complexity of the system response.

These observations have direct implications for model selection. The identified influence of off-axis flexibilities supports the relevance of adopting a triaxial flexibility representation. In contrast, simplified formulations such as Single VJM models, which account only for torsional flexibility about the motor axis, would neglect parameters shown here to have a noticeable impact on the response. As a result, such simplifications would affect the accuracy of the model. The triaxial formulation therefore appears to provide a more appropriate compromise between model fidelity and the ability to capture the dominant sensitivity trends highlighted in this study.

4 Global Methods

Global sensitivity analysis methods are characterised by the simultaneous variation of model input variables over their entire domain, as described by Buis [25]. These methods make it possible to identify the parameters that have the greatest influence on the system's response, while also capturing non-linear effects and interactions between variables. In the present work, the identification of parameter interactions is of particular importance, as optimisation procedures may lead to incorrect or non-unique parameter estimates when interdependencies between variables are neglected.

4.1 Improved Morris Analysis

The first method used is the *Improved Morris Analysis*, which is based on the classical *Morris Sensitivity Analysis* [27]. This approach is commonly used as a screening technique to identify negligible input variables, thereby reducing the dimensionality of the parameter space prior to the application of variance-based sensitivity methods [28]. Such variance-based methods, including Sobol's analysis, typically require a large number of model evaluations (on the order of 10^5) to ensure reliable estimates. The use of the Improved Morris Analysis is particularly relevant in the present study, as the model involves 44 input parameters and requires approximately 5.5 seconds per simulation. Since the computational cost of Sobol's sensitivity analysis increases rapidly with the number of parameters under consideration, it is advantageous to retain only the most influential variables. This preliminary screening step enables the subsequent variance-based analysis to be performed within a reasonable computational time while preserving the most relevant model dynamics.

The method is a one-at-a-time (OAT) screening method in which each dimension of the input parameter space of a model, collectively forming a hypercube. The range of each input parameter of the model is scaled to lie between 0 and 1. Each parameter range is then divided into a finite number of evenly spaced values, usually called p levels. Thus, the different levels are given by { 0, 1/(p-1), 2/(p-1), ..., 1 }. The procedure starts by selecting an initial set of parameter values from these p levels. From this starting point, the model is run several times. At each run, only one parameter is increased by a fixed amount, denoted by Δ, while all other parameters remain unchanged. The effect of this small change on the model output is called the elementary effect and is defined in Equation 4. For a model with k input parameters, this process requires k+1 model runs: one for the initial parameter set and one additional run for each parameter change. This sequence of k+1 simulations is referred to as a trajectory. In order to correctly explore the space of the parameters, several trajectories (n_{traj}) are created.

$$EE_{ij} = \frac{f(X_1, ..., X_i + \Delta, ..., X_k) - f(X_1, ..., X_i, ..., X_k)}{\Delta} \tag{4}$$

With :

- EE_{ij} : Elementary effects for the input factor i and the output variable j
- $Y = f(X_1, ..., X_k)$: The model
- X_i : Input parameter i
- k : The number of input parameters
- $\Delta : p/(2 * (p - 1))$: Variation of a parameter
- i : Parameter number
- j : Trajectory number

This allows us to determine some measures, μ_i (Equation 5), which assesses the importance of the parameter i on the output of the model, μ_i^* (Equation 6), the mean of the absolute values of the elementary effects of parameter i (improved measure of the μ from Morris analysis developed by Campolongo [29]) and σ_i (Equation 7), giving a measure of the interactions and non-linear effects of parameter i. Improves on Morris analysis have also been made by Sin et al. [30] in order to classify the parameters more accurately, without having to pay attention to different units.

$$\mu_i = \frac{1}{n_{traj}} \sum_{j}^{n_{traj}} EE_{ij} \tag{5}$$

$$\mu_i^* = \frac{1}{n_{traj}} \sum_{j}^{n_{traj}} |EE_{ij}| \tag{6}$$

$$\sigma_i = \sqrt{\frac{1}{n_{traj} - 1} \sum_{j}^{n_{traj}} (EE_{ij} - \mu_i)^2} \tag{7}$$

The values selected for the Morris sensitivity analysis settings are listed in Table 3. These values correspond to the higher end of the typical range used for this type of analysis, in order to improve the accuracy of the estimated elementary effects. Another critical consideration is the domain of the input parameters. To explore a broad and meaningful range of possible parameter values, the domain for input parameter i was chosen as [0.1,10].k_i, where k_i is the nominal value of the parameter. Consequently, a transformation is applied to map the normalized Morris sample values in the range [0,1].k_i to the simulation input range

[0.1,10].k_i. To ensure that the full parameter domain is sampled effectively, with a roughly equal probability of values falling below and above the nominal parameter, a logarithmic normalization is applied.

Table 3: Setting Values for the Morris Analysis

Setting	Value
n_{traj}	55
k	44
p	10

Figures 17 shows the distribution of the *p* values for the stiffness value of the 1st joint in the x direction and the same distribution after application of the logarithmic normalisation, added for all the trajectories. It shows that the entire domain is studied by the method and, after application of the logarithmic normalisation, about half of the time, the values will be under the nominal value, and the other half, above. The generation of the trajectories is done using an "optimization" option in which the sampling produces more trajectories (2000 in our simulations) and chooses the ones that, combined, cover the space in the most uniform way possible.

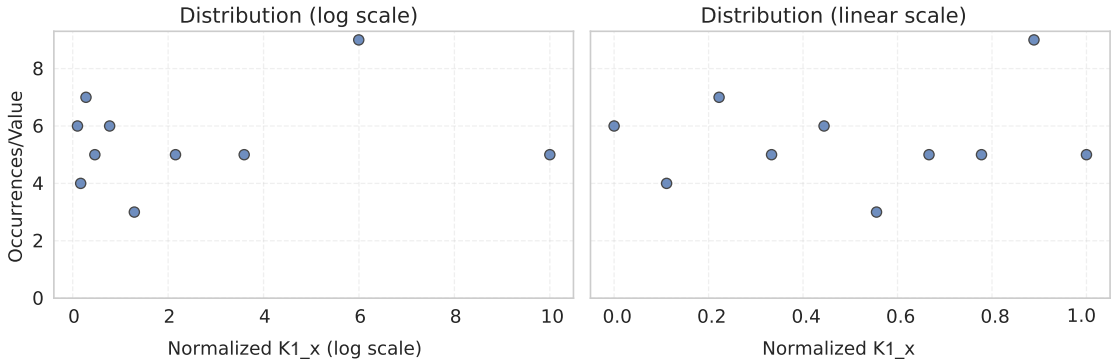


Fig. 17: Distribution of the values of $K1_x$ in the studied domain

The results obtained with this method for pose 170 are presented in Figure 18. The analysis identifies the same parameter as the most influential. Overall, similar trends are observed: the stiffness parameters exhibit a dominant influence, whereas the DVA has a negligible effect. Although the ranking of parameter importance differs, this discrepancy can be attributed to the differences in the computational approaches used in the OAT and Morris analyses. Despite these differences, both methods reveal consistent global trends. Figure 19 shows the ratio σ/μ^* of each parameter. The number of parameters make the graph difficult to read, this explains why only the names of the 10 most influent parameters are shown. However, the important information that can be retained is that almost all the parameters have this ratio > 1. This shows that they're non linear and probably interact with each other. This made it important to check for further studies, to determine which parameters are interacting together.

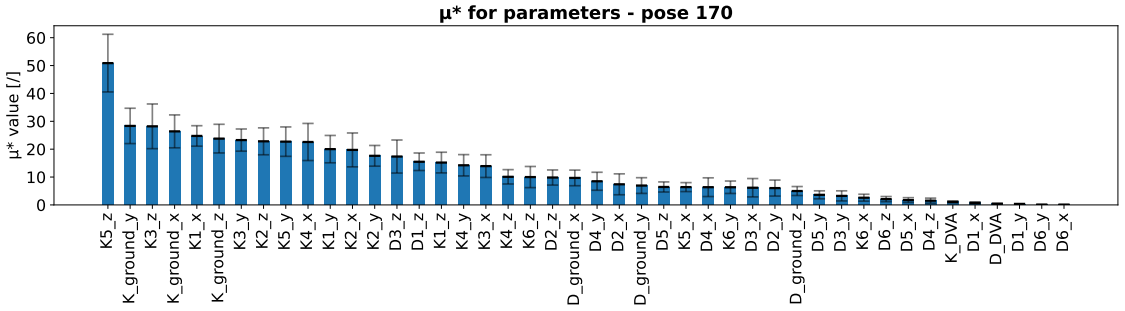


Fig. 18: μ^* values - pose 170

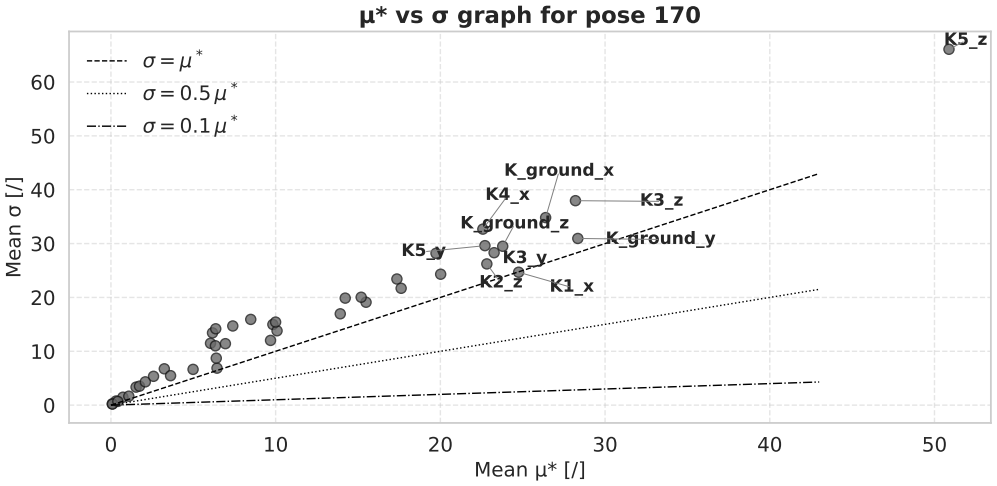


Fig. 19: $\sigma - \mu^*$ values - pose 170

The analysis given in Figure 20 shows the same trend as the OAT analysis for the influence of the planes, showing no real difference between the planes. However, the order of importance of the parameters is quite different. This might be due to the use of a different calculation method in the Morris analysis. As μ^* was developed in a proved method. This will be the index used to determine the order of importance of the parameters. Figures 21 and 23 show the evolution of the sensitivity of the system for the most important parameters along the X and Y directions. Comparing the results to the ones of the OAT analysis, it shows that, with a few exceptions, both methods agree on the most important parameters of the system. Overall, the evolution of the sensitivity of the parameters with the position is less smooth with Morris analysis. This could be resolved using more trajectories, at the cost of more simulation time. Important tendencies seem to be captured by Morris analysis (X direction : $K5_z$, $K5_y$, Y direction : $K5_z$, $K3_y$) while less important evolutions are not captured (X direction : $Kground_y$, $K3_z$, Y direction : $Kground_z$). The reasons behind this behaviour are probably linked to the way the μ^* compares to the mean value of the sum of the cost function values.

Figure 23 shows the evolution across the Y orientations of the mean point. It can be seen that the orientation with 0° seems to be less sensitive to changes in the values of the parameters, and that the more important is the angle, the more sensitive the model will be. This is true except for $K5_z$, which is more important for the neutral orientation. This kind of results are seen across the plane (checking for other TCP points). However, for rotations around X and Z, it is more difficult to find a pattern.

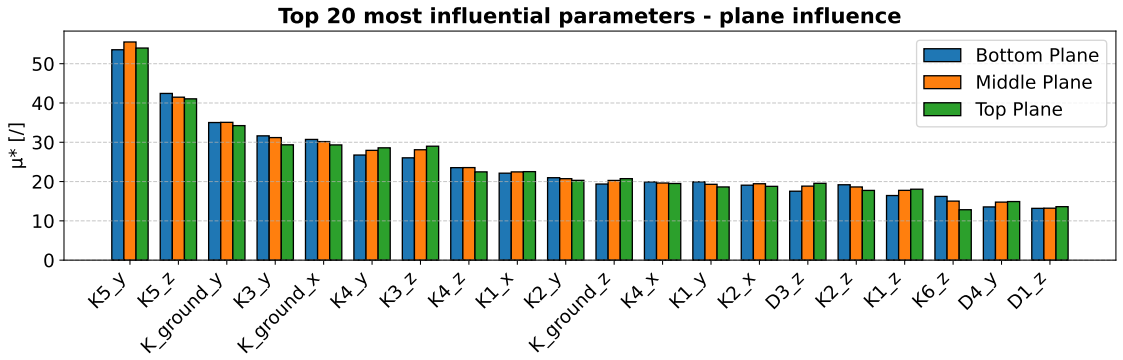


Fig. 20: Most influential parameters over the 3 planes studied

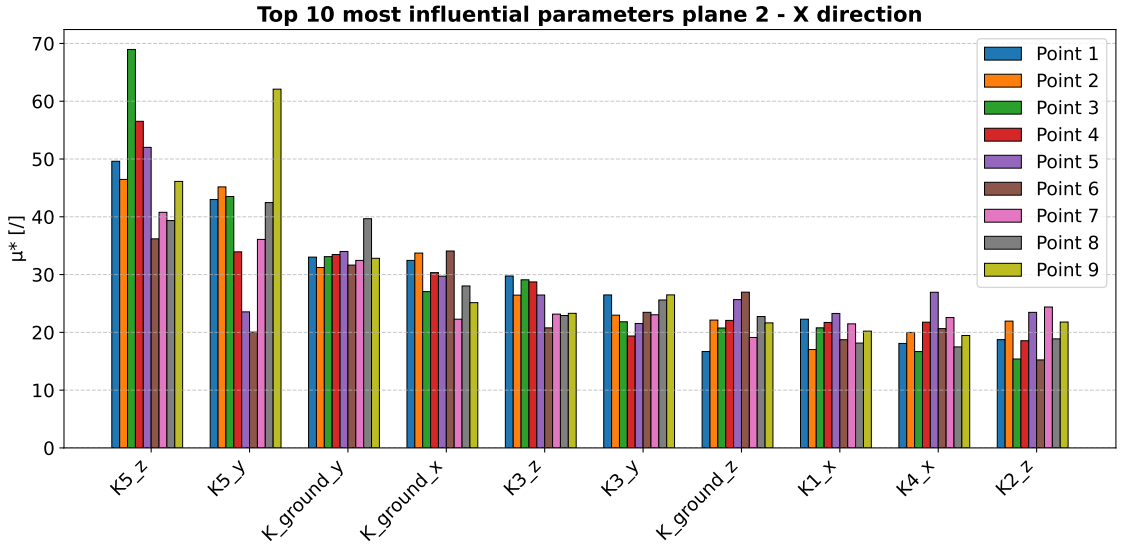


Fig. 21: Most influential parameters - Mean plane - X evolution - Morris

To resume this part on the Morris analysis, the results and observations are similar to what was seen with the OAT analysis, with a difference in the way the impact of parameters are calculated, which explains a difference in the order of influence of the parameters on the model. Morris analysis continues to show that some parameters have a negligible influence on the model (the DVA parameters, as well as the majority of damping parameters). Morris analysis brings also the confirmation that all parameters have a non-linear influence and are potentially interdependent. Consequently, it is necessary to study these potential dependencies.

4.2 Sobol analysis

To determine potential interdependencies between parameters, this study employs Sobol indices, a variance-based global sensitivity measure that quantifies how output uncertainty is attributed to input variations and their interactions [31]. This method uses different indices, the first order indices (Equation 8 (a)) represent the fraction of the output variance explained by variations in a single input parameter alone, averaged over the uncertainty in all other inputs. It therefore captures the direct contribution of that parameter to the model response. The second-order Sobol index (Equation 9) quantifies the contribution to output variance arising from the interaction between two input parameters, beyond their individual first-order effects, and thus reflects how pairs of parameters jointly influence the response (non additive effects). The total-order Sobol index (Equation 8 (b)) measures the overall contribution of a given input parameter, including both

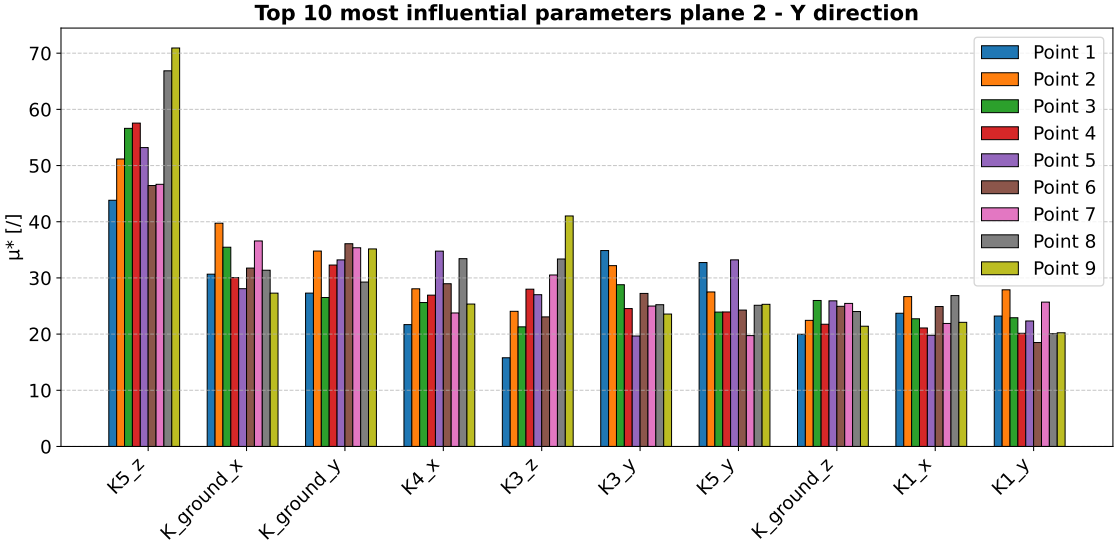


Fig. 22: Most influential parameters - Mean plane - Y evolution - Morris

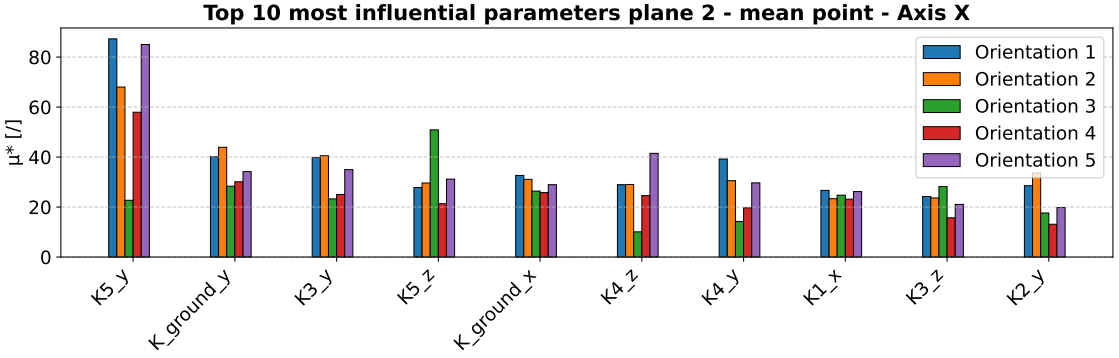


Fig. 23: Most influential parameters - comparison for the orientations around Y for centre point of the mean plane

its first-order effect and all higher-order interaction effects with other parameters. Consequently, while first-order indices identify parameters with strong individual influence, total-order indices reveal parameters that are important either on their own or through interactions, and second-order indices specifically highlight the strength of pairwise interactions within the system. The main hypothesis of this method is the independence of the parameters, which is respected by the use of a Latin Hypercube Sampling (LHS). The toolbox used for the calculation of the indices is SALib [32].

$$\text{(a)} \quad S_i = \frac{\mathrm{Var}_{X_i}(\mathbb{E}_{\mathbf{X}_{\sim i}}[Y \mid X_i])}{\mathrm{Var}(Y)} \qquad \text{(b)} \quad S_i^{\mathrm{T}} = \frac{\mathbb{E}_{\mathbf{X}_{\sim i}}(\mathrm{Var}_{X_i}[Y \mid \mathbf{X}_{\sim i}])}{\mathrm{Var}(Y)}. \tag{8}$$

$$S_{ij} = \frac{\mathrm{Var}_{X_i,X_j}\big(\mathbb{E}_{\mathbf{X}_{\sim ij}}[Y \mid X_i, X_j]\big) - \mathrm{Var}_{X_i}(\mathbb{E}_{\mathbf{X}_{\sim i}}[Y \mid X_i]) - \mathrm{Var}_{X_j}\big(\mathbb{E}_{\mathbf{X}_{\sim j}}[Y \mid X_j]\big)}{\mathrm{Var}(Y)} \tag{9}$$

Because the computation of Sobol sensitivity indices requires a large number of model evaluations, typically ranging from 10,000 to 100,000 depending on the number of input variables, a metamodel was developed to approximate the original model and enable significantly faster evaluations. The domain of the parameters is the same as in the Morris analysis, with the same distribution of the values of the parameters in the LHS.

The type of metamodel used is a Kriging metamodel (Matérn5/2) as it has been demonstrated that this type of model is the best for non-linear problems with no noise [33]. Kriging metamodels are cited along the most accurate models in general [34, 35]. The python library used for the metamodel is the SMT toolbox [36].

The training of the metamodel is done by taking an initial pool of n_{train} points, which is 60 times the number of variables fed to the metamodel, and calculating what the robot model would give as an output. Both the sets of parameters and the corresponding values of the cost function are fed to the model.

To verify the metamodel, several values are monitored and some thresholds have been determined. Firstly, 20% more points are used for testing compared to the number of training points. For this, 3 metrics are used, the RMSE error and the maximum error between the values predicted by the metamodel and the values determined with the robot model, as well as a metric called R^2 [37] defined by Equation 10. Only the last metric has a threshold, at 0.9, while the others are saved and monitored afterward to verify about any issue. A K-FOLD verification with 10 folds (Coded with Scikit-learn [38]) has also been used for further verification. The metrics used for the K-FOLD are the mean and standard deviation of the RMSE, R^2 and reduced chi-square statistic across the folds, as well as the maximum error. The thresholds have been put on the mean R^2 as 0.9 and on the reduced chi-square statistic at 1.5. The rest of the metrics are verified afterwards by hand to check if the model is consistent. If the verification shows that the metamodel does not fit the function well enough, more training points are added by selecting points in an LHS.

$$R^2 = 1 - \frac{\sum_{i=0}^{n_{test}} (Y_i - \hat{Y}_i)^2}{\sum_{i=0}^{n_{test}} (Y_i - \overline{Y}_{train})^2} \tag{10}$$

With :

- n_{test} : The number of test points of the metamodel
- Y_i : The value of the cost function for the test point *i* with the robot model
- $\hat{Y}_i$: The prediction of the cost function for the test point *i* with the metamodel
- $\overline{Y}_{train}$: The mean value of the cost function across the training points with the robot model

The metamodel was applied to pose 170 using subsets of six variables at a time in order to investigate potential coupling effects between flexibilities. Four independent runs of the same metamodel, each with different sets of input parameters, were performed for both the ground and the first joint stiffnesses and showed consistent results, confirming the robustness of the approach. Representative results from one of the runs are reported in Table 4. The sum of the first-order Sobol indices is 0.91, compared to 1.13 for the total-order indices, yielding a difference of 0.22 that quantifies the contribution of interaction effects to the output variance. This relatively small value confirms that the system response is dominated by the direct effects of individual parameters, with interactions accounting for less than a quarter of the variance. The proximity of the first and total order sums indicates a near-additive behavior, meaning that parameters can be identified largely independently of one another, a finding that supports the multipass identification strategy discussed in the conclusion.

It should be noted that this analysis was limited to subsets of six parameters due to computational constraints. Constructing a reliable Kriging metamodel with six parameters required approximately three hours of computation, whereas extending the model to nine parameters increased this cost to approximately three days. Beyond this, metamodel accuracy deteriorates as the input dimensionality increases unless the training set is substantially enlarged, making a full 44-parameter Sobol analysis intractable without dedicated high-performance computing resources. This limitation is acknowledged, and the subset-based approach was designed to maximize coverage of physically meaningful parameter combinations while remaining computationally feasible.

The metamodel was evaluated across all possible pairwise joint combinations, to get all the combinations of second order indices. For most joint pairs, including the ground and first joint configuration, second-order

Sobol indices were found to be negligible, with a maximum observed value for the interaction between $K1_y$ and Kgd_x of 0.027 $\pm$ 0.004 and most other indices remaining below 0.01. These results are consistent with the independent sampling ensured by the Latin Hypercube Sampling procedure and confirm the predominantly additive character of the system response across the majority of parameter combinations. The metamodel for the results given in Table 4 have the following values for the validation : $R^2 = 0.946$, $R^2_{KFOLD} = 0.911$ and chi-square = 1.293. The other runs of the metamodel showed similar results.

Two notable exceptions were however identified: the parameter pairs $(K3_z, K4_x)$ and $(K3_z, K5_z)$, for which second-order Sobol indices reached 28.20 ± 0.01% and 13.70 ± 0.005% respectively. The first elevated interaction effect can be attributed to the geometric relationship between joints 3 and 4 introduced by the kinematic chain. The reference frame of joint 4 is reoriented with respect to that of the elbow by a rotation of $\pi/2$ around the y-axis, which maps the nominal rotation axis of motor 4 onto the x-axis of the elbow frame. As a result, the torsional flexibility $K3_z$, acting around the z-axis of the elbow frame, and the flexibility $K4_x$, acting around the reoriented x-axis of joint 4, share a common geometric dependency: a perturbation of $K3_z$ alters the effective orientation of the reference frame in which $K4_x$ is expressed, creating a coupled influence on the response of the system that cannot be captured by first-order effects alone. It is also noteworthy that the nominal values of $K3_z$ and $K4_x$ are of similar magnitude, 2.76x10^6 and 2.96×1010^6 Nm/rad respectively, as shown in Table 2, meaning that perturbations of equal relative amplitude produce effects of comparable scale, which may amplify the observable interaction in the cost function. A similar geometric argument applies to the second pair. The successive frame transformations accumulated along the kinematic chain between the elbow and joint 5 result in the z-axis of joint 5's local frame retaining a significant projection onto the z-axis of the elbow frame, maintaining a partial alignment between the two springs, in the nominal pose 170. This propagated geometric dependency explains the observed second-order interaction of 13.70%. From an identification standpoint, these two interacting pairs should be treated as coupled and estimated jointly, forming a natural exception to the otherwise predominantly additive parameter structure of the model. For all other joint combinations, second-order indices remained below a few percent, confirming that the multipass identification strategy proposed in Section 5 remains valid for the remaining parameters.

The predominantly additive behavior observed in the Sobol analysis aligns with the high σ/μ^* ratios seen in the Morris analysis. The Morris method captures the nonlinear effects of individual parameters over a wide range, while the Sobol indices show that interactions between parameters remain relatively small. Still, the combined effect of these minor interactions is enough to produce the elevated σ/μ^* ratios reported by Morris.

Table 4: Sobol's analysis results

	$K1_x$	$K1_y$	$K1_z$	Kgd_x	Kgd_y	Kgd_z
S_i	0.04	0.09	0.09	0.18	0.14	0.37
S_i^T	0.07	0.14	0.12	0.23	0.17	0.40

An additional analysis was conducted to assess the identifiability of the parameters using the full (real) model. Profile likelihoods were computed by varying two parameters at a time, enabling straightforward visualization of the resulting landscapes. The results, presented in Figures 24, indicate that for two parameter pairs, the profile likelihood exhibits a single minimum. This suggests that, in these cases, standard optimization methods are expected to reliably recover the true parameter values. However, this conclusion is not expected to generalize to higher-dimensional parameter spaces, where more complex likelihood landscapes may arise, including multiple local minima or flat regions. A comprehensive exploration of these higher-dimensional effects is computationally prohibitive and therefore was not performed over the entire parameter domain considered.

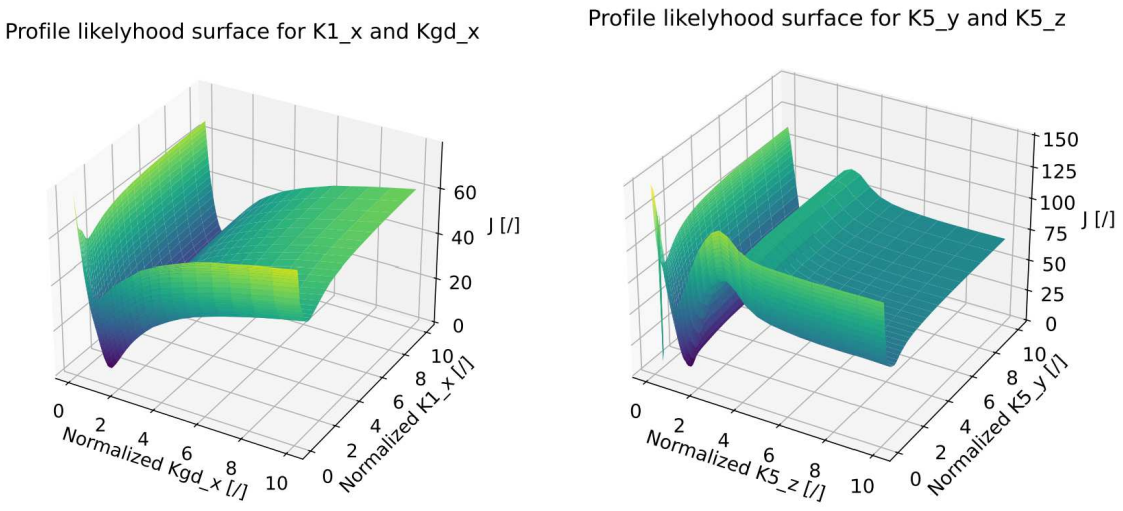


Fig. 24: Profile likelyhood for two pairs of parameters

5 Conclusions

This paper presented a comprehensive sensitivity analysis of the elastic parameters of a flexible 6-DOF industrial robot incorporating triaxial joint flexibility, conducted systematically across 351 configurations spanning both position and tool orientation within the operational workspace. Three complementary sensitivity methods were applied : One-At-a-Time, Improved Morris, and Sobol variance decomposition via a Kriging metamodel. Their results were found to be mutually consistent, strengthening the reliability of the conclusions drawn.

The OAT analysis demonstrated that the stiffness parameters dominate the system response across all configurations, while most of the damping coefficients and DVA parameters exert a negligible influence and may therefore be assigned fixed values during identification without significant loss of accuracy. A key practical outcome is that a parameter identified as influential at one workspace location remains influential throughout the studied workspace, regardless of tool orientation. This pose-consistency result implies that a single sensitivity-informed parameter ranking can guide identification strategies throughout the operational range, avoiding the need for pose-specific analyses. Furthermore, the analysis confirmed that off-axis flexibilities, which are absent from simpler Single VJM formulations, carry non-negligible sensitivity weight, providing quantitative justification for the adoption of the triaxial model over simplified alternatives.

The Morris analysis corroborated these findings at the global level, confirming the dominant role of stiffness parameters and the negligible contribution of DVA parameters across the full configuration space. It further indicated that parameters exhibit nonlinear behavior and are potentially interdependent, motivating the Sobol analysis via a surrogate model.

Variance decomposition via the Kriging metamodel revealed that the system response is predominantly additive, with the sum of first-order Sobol indices reaching 0.91 against 1.13 for total-order indices. Pairwise interactions were found to be negligible for the vast majority of parameter combinations, with two notable exceptions: the pairs $(K3_z, K4_x)$ and $(K3_z, K5_z)$, for which second-order indices reached 28% and 14% respectively. These interactions were traced back to specific geometric dependencies in the kinematic chain and positioning of the robot, and are therefore structural rather than incidental. Profile likelihood surfaces confirmed the existence of a single identifiable minimum for these coupled pairs, suggesting that joint estimation remains tractable.

These findings collectively support a structured multipass identification strategy for FRF-based model updating. Parameters should be optimized in successive batches ordered from most to least influential, with batch sizes not exceeding six, as interactions among groups of this size were shown to be weak. A natural first batch would consist of the ground stiffnesses and the stiffness parameters of joint 5, which were

consistently identified as the most influential across the workspace. The two geometrically coupled pairs $(K3_z, K4_x)$ and $(K3_z, K5_z)$ should be treated as exceptions and estimated jointly rather than sequentially. Damping parameters, given their weak and consistent sensitivity behavior, may either be fixed at physically motivated values or estimated in a final batch once the dominant stiffness parameters have been identified. If necessary, a multi-objective formulation dividing the cost function across frequency bands could further improve robustness.

Statements and Declarations

Competing interests The authors have no competing interests to declare that are relevant to the content of this article.

Author contributions H.D. did the Conceptualization, Model Development, Methodology, Formal Analysis and Investigation as well as the Writing - Original Draft Preparation; V.D., E.R. and B.O. participated in the Initial Model Development, the Review and Editing as well as the Supervision.

REFERENCES

[1] A. Verl, A. Valente, S. Melkote, C. Brecher, E. Ozturk, L. T. Tunc, Robots in machining, CIRP Annals 68 (2) (2019) 799–822. doi:10.1016/j.cirp.2019.05.009.

[2] H. Dantinne, V. Dambly, O. Verlinden, F. Ducobu, B. Olivier, E. Riviere-Lorphevre, Performance and efficiency of co-simulation for milling operations in robotic machining, Procedia CIRP 133 (20th CIRP Conference on Modeling of Machining Operations in Mons) (2025) 114–119. doi:10.1016/j.procir.2025.02.021.

[3] A. Blomdell, G. Bolmsjo, T. Brogardh, P. Cederberg, M. Isaksson, R. Johansson, M. Haage, K. Nilsson, M. Olsson, T. Olsson, A. Robertsson, Jianjun Wang, Extending an industrial robot controller, IEEE Robotics & Automation Magazine 12 (3) (2005) 85–94. doi:10.1109/MRA.2005.1511872.

[4] A. Klimchik, Y. Wu, S. Caro, B. Furet, A. Pashkevich, Accuracy Improvement of Robot-Based Milling Using an Enhanced Manipulator Model, in: M. Ceccarelli, V. A. Glazunov (Eds.), Advances on Theory and Practice of Robots and Manipulators, Springer International Publishing, Cham, 2014, pp. 73–81. doi:10.1007/978-3-319-07058-2_9.

[5] H. N. Huynh, Robotic machining: Development and validation of a numerical model of robotic milling to optimise the cutting parameters, Ph.D. thesis, UMONS (2019).

[6] S. Sampath, P. Duraisamy, A. M., A. Karthikeyan, K. Rajagopal, Effect of nonlinear stiffness on single link flexible joint robotic manipulator and its control, International Journal of Non-Linear Mechanics 163 (2024) 104730. doi:10.1016/j.ijnonlinmec.2024.104730.

[7] A. Klimchik, B. Furet, S. Caro, A. Pashkevich, Identification of the manipulator stiffness model parameters in industrial environment, Mechanism and Machine Theory 90 (2015) 1–22. doi:10.1016/j.mechmachtheory.2015.03.002.
URL https://linkinghub.elsevier.com/retrieve/pii/S0094114X15000397

[8] E. Paul, R. A. Boby, H. Krishnaswamy, A. Klimchik, Enhanced lumped stiffness model for industrial robots under multi-axial loading: Trade-off between the model complexity and positional accuracy, Mechanism and Machine Theory 214 (2025) 106133. doi:10.1016/j.mechmachtheory.2025.106133.
URL https://linkinghub.elsevier.com/retrieve/pii/S0094114X25002228

[9] T. Cvitanic, V. Nguyen, S. N. Melkote, Pose optimization in robotic machining using static and dynamic stiffness models, Robotics and Computer-Integrated Manufacturing 66 (2020) 101992. doi:10.1016/j.rcim.2020.101992.

[10] J. Gotlih, T. Karner, K. Gotlih, M. Brezocnik, Experiment Based Structural Stiffness Calibration of a Virtual Robot Model, in: B. Katalinic (Ed.), DAAAM International Scientific Book, 1st Edition, Vol. 17, DAAAM International Vienna, 2018, pp. 131–140. doi:10.2507/daaam.scibook.2018.12.

[11] T. Tsumugiwa, Y. Fukui, R. Yokogawa, Compliance measurement for the Mitsubishi PA-10 robot, Advanced Robotics 28 (14) (2014) 919–928. doi:10.1080/01691864.2014.899159.

[12] R. A. Boby, Identification of elasto-static parameters of an industrial robot using monocular camera, Robotics and Computer-Integrated Manufacturing 74 (2022) 102276. doi:10.1016/j.rcim.2021.102276.

[13] Y. Yin, D. Gao, Y. Lu, C. Zhao, G. Li, K. Deng, In-situ robot joint stiffness identification using an eye-in-hand camera with optimal measurement pose selection, Measurement 253 (2025) 117579. doi:10.1016/j.measurement.2025.117579.

[14] M. Neubauer, H. Gattringer, A. Müller, A. Steinhauser, W. Höbarth, A two-stage calibration method for industrial robots with joint and drive flexibilities, Mechanical Sciences 6 (2) (2015) 191–201. doi:10.5194/ms-6-191-2015.

[15] C. Ye, J. Yang, H. Ding, High-accuracy prediction and compensation of industrial robot stiffness deformation, International Journal of Mechanical Sciences 233 (2022) 107638. doi:10.1016/j.ijmecsci.2022.107638.

[16] R. Wang, F. Li, J. Niu, Y. Sun, Prediction of pose-dependent modal properties and stability limits in robotic ball-end milling, Robotics and Computer-Integrated Manufacturing 75 (2022) 102307. doi:10.1016/j.rcim.2021.102307.

[17] H. Chen, K. Ahmadi, Estimating pose-dependent FRF in machining robots using multibody dynamics and Gaussian Process Regression, Robotics and Computer-Integrated Manufacturing 77 (2022) 102354. doi:10.1016/j.rcim.2022.102354.

[18] H. N. Huynh, E. Rivière-Lorphèvre, O. Verlinden, Multibody modelling of a flexible 6-axis robot dedicated to robotic machining, Lisbon, 2018.

[19] J. Denavit, R. S. Hartenberg, A Kinematic Notation for Lower-Pair Mechanisms Based on Matrices, Journal of Applied Mechanics 22 (2) (1955) 215–221. doi:10.1115/1.4011045.

[20] H. N. Huynh, Y. Altintas, Modeling the Dynamics of Five-Axis Machine Tool Using the Multibody Approach, Journal of Manufacturing Science and Engineering 143 (2) (2021) 021012. doi:10.1115/1.4048854.

[21] O. Verlinden, H. N. Huynh, G. Kouroussis, E. Rivière-Lorphèvre, Modelling of flexible bodies with minimal coordinates by means of the corotational formulation, Multibody System Dynamics 42 (4) (2018) 495–514. doi:10.1007/s11044-017-9609-0.

[22] H. N. Huynh, H. Assadi, V. Dambly, E. Rivière-Lorphèvre, O. Verlinden, Direct method for updating flexible multibody systems applied to a milling robot, Robotics and Computer-Integrated Manufacturing 68 (2021) 102049. doi:10.1016/j.rcim.2020.102049.

[23] E. Abele, S. Rothenbücher, M. Weigold, Cartesian compliance model for industrial robots using virtual joints, Production Engineering 2 (3) (2008) 339–343. doi:10.1007/s11740-008-0118-0.

[24] J.-B. Blanchard, B. Iooss, Introduction à l'analyse de sensibilité de modèles numériques.
URL https://uranie.cea.fr/pdf_files/Sensitivity.pdf

[25] S. Buis, Analyse de sensibilité des modèles de simulation (2014).
URL https://www.eccorev.fr/IMG/pdf/Sensibilite_SBuis.pdf

[26] M. Hou, H. Cao, J. Shi, Y. Guo, An industry-oriented digital twin model for predicting posture-dependent FRFs of industrial robots, Mechanical Systems and Signal Processing 212 (2024) 111251. doi:10.1016/j.ymssp.2024.111251.
URL https://www.sciencedirect.com/science/article/pii/S0888327024001493

[27] M. D. Morris, Factorial Sampling Plans for Preliminary Computational Experiments, Technometrics 33 (2) (1991) 161–174. doi:10.1080/00401706.1991.10484804.

[28] O. Tsvetkova, T. B. Ouarda, A review of sensitivity analysis practices in wind resource assessment, Energy Conversion and Management 238 (2021) 114112. doi:10.1016/j.enconman.2021.114112.

[29] F. Campolongo, J. Cariboni, A. Saltelli, An effective screening design for sensitivity analysis of large models, Environmental Modelling & Software 22 (10) (2007) 1509–1518. doi:10.1016/j.envsoft.2006.10.004.

[30] G. Sin, K. V. Gernaey, Improving the Morris method for sensitivity analysis by scaling the elementary effects, in: Computer Aided Chemical Engineering, Vol. 26, Elsevier, 2009, pp. 925–930. doi:10.1016/S1570-7946(09)70154-3.

[31] M. Tosin, A. M. A. Côrtes, A. Cunha, A Tutorial on Sobol' Global Sensitivity Analysis Applied to Biological Models, in: F. A. B. Da Silva, N. Carels, M. Trindade Dos Santos, F. J. P. Lopes (Eds.), Networks in Systems Biology, Vol. 32, Springer International Publishing, Cham, 2020, pp. 93–118. doi:10.1007/978-3-030-51862-2_6.

[32] J. Herman, W. Usher, SALib: An open-source Python library for Sensitivity Analysis, The Journal of Open Source Software 2 (9) (2017) 97. doi:10.21105/joss.00097.

[33] M. R. Kianifar, F. Campean, Performance evaluation of metamodelling methods for engineering problems: towards a practitioner guide, Structural and Multidisciplinary Optimization 61 (1) (2020) 159–186. doi:10.1007/s00158-019-02352-1.

[34] B.-S. Kim, Y.-B. Lee, D.-H. Choi, Comparison study on the accuracy of metamodeling technique for non-convex functions, Journal of Mechanical Science and Technology 23 (4) (2009) 1175–1181. doi:10.1007/s12206-008-1201-3.

[35] Y. Li, S. Ng, M. Xie, T. Goh, A systematic comparison of metamodeling techniques for simulation optimization in Decision Support Systems, Applied Soft Computing 10 (4) (2010) 1257–1273. doi:10.1016/j.asoc.2009.11.034.

[36] P. Saves, R. Lafage, N. Bartoli, Y. Diouane, J. Bussemaker, T. Lefebvre, J. T. Hwang, J. Morlier, J. R. Martins, SMT 2.0: A Surrogate Modeling Toolbox with a focus on hierarchical and mixed variables Gaussian processes, Advances in Engineering Software 188 (2024) 103571. doi:10.1016/j.advengsoft.2023.103571.

[37] H. Amiri, U. C. Kucuk, O. Kucukoglu, Y. Kuscu, O. Ozdemır, Evaluating Diverse Meta-modeling Approaches for Predicting Performance Characteristics of a Twin Air Intake Based on Experimental Data, Journal of Applied Fluid Mechanics 18 (4) (Jun. 2025). doi:10.47176/jafm.18.6.3171.

[38] F. Pedregosa, G. Varoquaux, A. Gramfort, V. Michel, B. Thirion, O. Grisel, M. Blondel, P. Prettenhofer, R. Weiss, V. Dubourg, J. Vanderplas, A. Passos, D. Cournapeau, M. Brucher, M. Perrot, E. Duchesnay, Scikit-learn: Machine Learning in Python 12 (2012) 2825–2830.